



# Lattice-preferred orientation and microstructure of peridotites from ODP Hole 1274A (15°39'N), Mid-Atlantic Ridge: Testing models of mantle upwelling and tectonic exhumation

Kay L. Achenbach<sup>a,\*</sup>, Michael J. Cheadle<sup>a</sup>, Ulrich Faul<sup>b</sup>, Peter Kelemen<sup>c</sup>, Susan Swapp<sup>b</sup>

<sup>a</sup> Department of Geology and Geophysics, Dept. 3006, 1000 University Ave., University of Wyoming, Laramie, WY 82072, USA

<sup>b</sup> Department of Earth Sciences, Boston University, 675 Commonwealth Avenue, Boston, MA 02215, USA

<sup>c</sup> Lamont-Doherty Earth Observatory, 61 Route 9W-PO Box 1000, Palisades, NY 10964-8000, USA

## ARTICLE INFO

### Article history:

Received 30 April 2010

Received in revised form 6 October 2010

Accepted 31 October 2010

Available online 3 December 2010

Editor: L. Stixrude

### Keywords:

mantle upwelling  
mid-ocean ridge processes  
lattice-preferred orientation  
electron backscatter diffraction  
abyssal peridotites

## ABSTRACT

Eleven harzburgites and one dunite from Ocean Drilling Program Leg 209 Hole 1274A preserve high-temperature mantle textures. Electron backscatter diffraction (EBSD) analysis shows moderately developed crystal lattice preferred orientations (LPOs) in olivine and orthopyroxene (M-indices  $\approx 0.1$ ) indicative of crystal-plastic deformation at  $\sim 1250$  °C. These rocks preserve a protogranular texture with a weak olivine foliation, a very weak or absent orthopyroxene foliation that may be decoupled from the orthopyroxene LPO, and minor interstitial clinopyroxene and spinel. Olivine grain size distributions, along with melt-related microstructures in orthopyroxene, clinopyroxene and spinel suggest that high-temperature deformation textures have been overprinted by pervasive post-deformation melt-rock interaction. Paleomagnetic data constrain the olivine [100] axes to be subhorizontal and oriented at low angle ( $\leq 28.6^\circ \pm 10.6^\circ$ ) to the ridge axis at the onset of serpentinization. This orientation is consistent with either complex 3-D mantle upwelling or 2-D mantle upwelling coupled with complex 3-D tectonic emplacement to the seafloor.

© 2010 Elsevier B.V. All rights reserved.

## 1. Introduction

A fundamental characteristic of mid-ocean ridges is the behaviour of the mantle as it upwells beneath the ridge axis. Two end-member models of mantle upwelling geometry have emerged. The first, a two-dimensional (2-D) model, involves a mantle which upwells passively in response to plate separation. Upwelling is uniform along the ridge axis. Subsequent to corner flow (the transition from vertical upwelling to horizontal spreading), the mantle flows perpendicularly away from the ridge axis. The alternative model is three-dimensional (3-D), involving mantle upwelling that may be actively driven by buoyancy. Along the ridge axis, upwelling is focused at ridge segment centers. Subsequent to corner flow the mantle flows away from ridge segment centers in a radial pattern before transitioning to a passive 2-D geometry at some distance from the ridge axis. 3-D upwelling has been invoked at slow-spreading ridges to explain seismic (Tolstoy et al., 1993; Tucholke et al., 1997), gravity (e.g., Kuo and Forsyth, 1988; Lin et al., 1990) and geological (Dick, 1989; Whitehead et al., 1984) observations suggestive of thicker crust and abundant basalt at ridge

segment centers and thinner crust with exposed peridotite and gabbro near ridge segment ends. At fast-spreading ridges, recent seismic tomography experiments have observed low-velocity zones beneath the East Pacific Rise (Toomey et al., 2007) and the Gulf of California (Wang et al., 2009) thought to be regions of 3-D upwelling and melting, and the mantle section of the Oman Ophiolite preserves structures indicative of mantle diapirs or 3-D flow (Ceuleneer et al., 1988; Jousset et al., 1998; Nicolas and Rabinowicz, 1984; Nicolas and Violette, 1982). Some seismic anisotropy observations have implied that mantle flow directions may be skewed from ridge-perpendicular, by  $\sim 9^\circ$  at the East Pacific Rise (Toomey et al., 2007) and by  $\sim 38^\circ$  at the Mid-Atlantic Ridge (Dunn et al., 2005). The cause of this apparent skew is not certain, though it may be due to ridge migration relative to the hotspot frame (Dunn et al., 2005) or changing patterns of global mantle flow (Toomey et al., 2007). Both of these hypotheses essentially invoke a 2-D mantle pattern that has been rotated with respect to the surface tectonics, although both Dunn et al. (2005) and Toomey et al. (2007) report segment-center enhanced melt delivery, and thus do not preclude the possibility of a superimposed 3-D pattern with ridge-parallel flow below the resolution of the anisotropy observations.

The applicability of the 3-D upwelling model to slow-spreading mid-ocean ridges has yet to be shown conclusively. Ceuleneer and Cannat (1997) found azimuthally heterogeneous olivine [100] axes oriented at an oblique angle to the ridge axis in peridotites drilled at Ocean Drilling

\* Corresponding author. Present address: Department of Earth Sciences, Durham University, Science Labs, Durham, DH1 3LE, UK.

E-mail addresses: [kay.achenbach@durham.ac.uk](mailto:kay.achenbach@durham.ac.uk) (K.L. Achenbach), [cheadle@uwyo.edu](mailto:cheadle@uwyo.edu) (M.J. Cheadle), [ufaul@bu.edu](mailto:ufaul@bu.edu) (U. Faul), [peterk@ldeo.columbia.edu](mailto:peterk@ldeo.columbia.edu) (P. Kelemen), [swapp@uwyo.edu](mailto:swapp@uwyo.edu) (S. Swapp).

Program (ODP) Site 920 in the MARK area. This study was limited by the technical difficulty of measuring olivine and orthopyroxene crystal orientations prior to the advent of the electron backscatter diffraction (EBSD) technique and by structural reorientations that later paleomagnetic work (Lawrence et al., 2002) suggested may not have accounted for *in situ* deflections of the paleomagnetic vector from true north.

ODP Leg 209 (Kelemen et al., 2004) identified the Fifteen-Twenty Fracture Zone (FTFZ) area of the Mid-Atlantic Ridge (MAR) as an ideal location for testing models of mantle upwelling. The MAR from 14°–16°N to the north and south of the FTFZ has extensive outcrops of peridotites and gabbros on both sides of the axial valley (Kelemen et al., 2004 and references therein). Two “bull’s-eye” gravity lows centered at ~14°20’N and 16°00’N may be magmatic centers of ridge segments, zones at which melt delivery and/or mantle upwelling may be focused in three dimensions (Escartin and Cannat, 1999; Fujiwara et al., 2003). The full spreading rate of the ridge is ~25 mm/year, and the FTFZ offsets the ridge by ~200 km (Fujiwara et al., 2003).

ODP Leg 209 drilled 8 sites to the north and south of the FTFZ. Hole 1274A (Fig. 1) was the only hole that recovered peridotites with a sufficient quantity of unserpentinized olivine to assess mantle deformation. Located at 15°39’ ~31 km north of the fracture zone,

Hole 1274A was drilled in the western flank of the rift valley wall, and is ~6 km north of a non-transform discontinuity (Fujiwara et al., 2003). Hole 1274A penetrated to a total depth of 155.8 m below seafloor (mbsf) with ~22% total recovery (Kelemen et al., 2004). Of the total rock recovered from Hole 1274A, ~77% was harzburgite, ~20% dunite, and ~3% gabbro (Fig. 1). Additionally, from ~95–145 mbsf the recovered cores contained some intervals of serpentinite mud and breccia that were interpreted to be fault gouge; rock recovered from this portion of the core is highly to completely altered. On the thin-section scale some peridotite samples contain over 50% of the unaltered, original mantle mineralogy with some unaltered patches up to a few mm in diameter, making these among the freshest oriented peridotites ever recovered from *in situ* ocean crust. Shipboard analysis revealed that the peridotites of Hole 1274A are highly depleted harzburgites that preserve weakly deformed (pro-granular) mantle textures (Kelemen et al., 2004).

Subsequent studies confirm the depleted nature of the peridotites; this composition is the result of considerable melting, either related to the present-day upwelling (Godard et al., 2008) or resulting from an ancient depletion event (Harvey et al., 2006; Seyler et al., 2007; Suhr et al., 2008). Textural analysis of the Hole

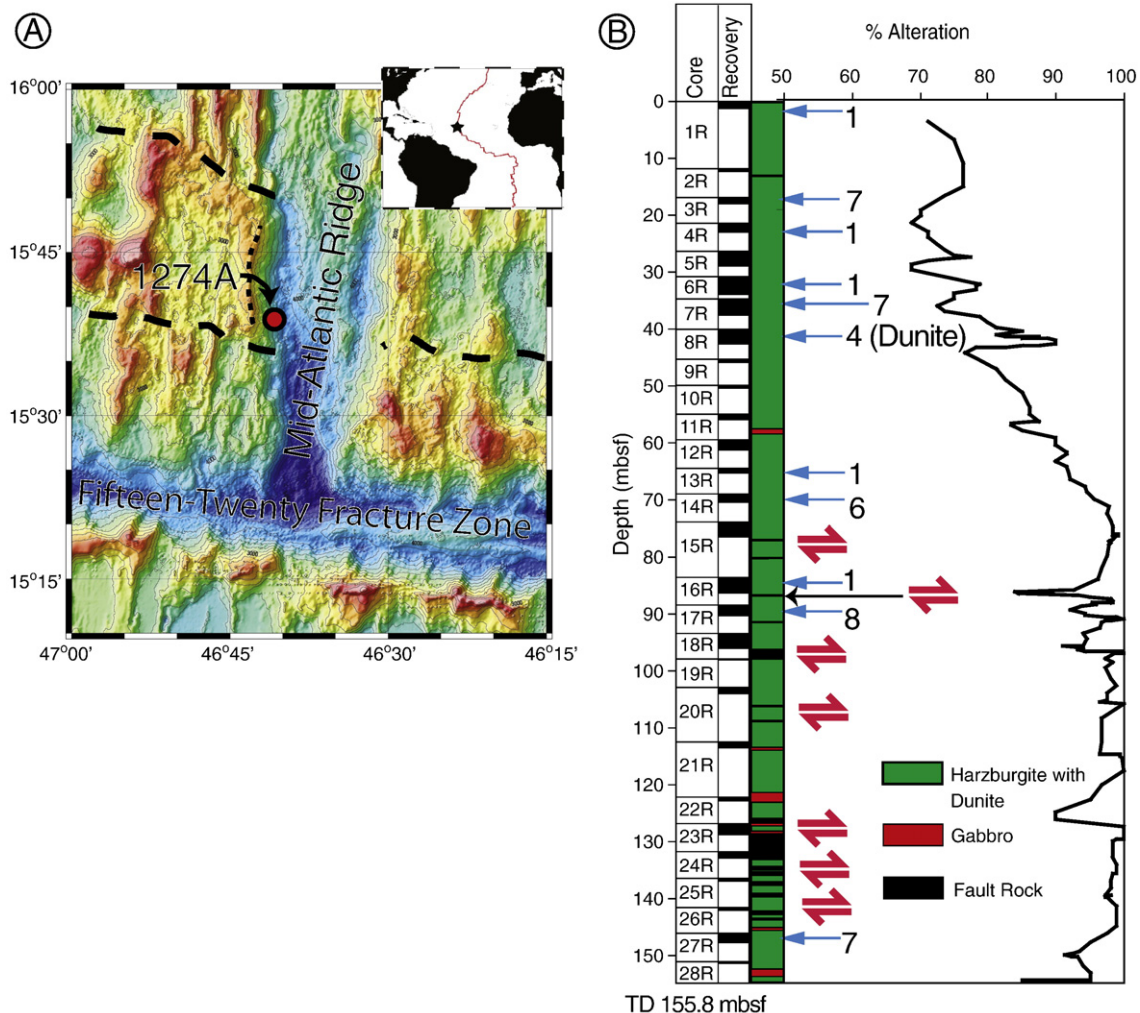


**Fig. 1.** A) Location of Hole 1274A, Ocean Drilling Program Leg 209. The heavy dashed lines indicate the interpreted non-transform discontinuities of Fujiwara et al. (2003). The fine dashed line indicates the fault scarp discussed in the text (Hole 1274A lies at the base of this scarp). Bathymetry is from Fujiwara et al. (2003). B) Diagram showing the lithology and recovery of ODP Hole 1274A. The column labeled “Core” indicates the core number. The column labeled “Recovery” indicates the amount of rock recovered from a given segment of core; black indicates recovered rock as a percentage of each core segment. The colored column indicates the rock type recovered from the core segment. Jagged black line indicates alteration downhole. In showing rock type and alteration in this figure, the recovered rock is scaled to the entire length of the core segment, although there is no constraint on the absolute depth of recovered rock within a given core segment (from Kelemen et al., 2004). Arrows with numbers indicate the location of samples and number of thin sections used in this study. Red arrow symbols indicate zones of interpreted faulting.

1274A peridotites (Seyler et al., 2007; Suhr et al., 2008) showed evidence for pervasive melt-rock interaction. Garces and Gee (2007) used paleomagnetism to show that the Hole 1274A peridotites, along with the rest of the rocks drilled during Leg 209, experienced considerable tectonic rotations.

The aim of this study is to characterize the microstructural and crystallographic fabrics of the Hole 1274A peridotites. We use the present-day orientation of olivine crystal lattice-preferred orientation (LPO) within the oceanic lithosphere to constrain the geometry of high-temperature mantle flow and low-temperature tectonic emplacement of mantle rocks to the seafloor on the MAR at 15°39'N.

## 2. Methods

Throughout this study, we used only samples which we could be sure were subject to the fewest uncertainties, both in size and orientation. A summary of samples, and the analyses performed on each, is shown in Table S1 in Supplementary Materials.

### 2.1. Microstructures

The original microstructure of these peridotites was reconstructed to obtain a complete picture of the pre-alteration grain-scale relationships of the original mantle minerals (Fig. 2). This was accomplished by manual tracing of the grain boundaries on high-

resolution digital images (3200 dpi). Where grain boundaries in olivine were not observable because of alteration, extinction angles and electron backscatter diffraction (EBSD) data were used to constrain the location of the original grain boundaries. Grain boundaries were defined when adjacent crystals had an angular mismatch of  $>10^\circ$ . Serpentine and disseminated opaque phases (assumed to be magnetite) were assigned to original olivine; serpentine “bastite” pseudomorphs were assigned to original orthopyroxene; opaque pseudomorphs after spinel were assigned to original spinel; clinopyroxene is unaltered. Veins and highly altered regions where grain boundaries could not be located were not included. The complete pre-alteration microstructure of 19 thin sections from three rocks was reconstructed. Because bastite pseudomorphs are easily distinguishable from completely serpentinized olivine, we reconstructed the orthopyroxene microstructure from 10 additional thin sections in two highly altered rocks (three thin sections from rock 027 and seven thin sections from rock 017).

These reconstructed images were used to calculate accurate estimates of grain size and shape-preferred orientation (SPO) by fitting equal-area ellipses and circles to each grain using the software ImageJ (Rasband, 1997–2007). Grains with unconstrained boundaries, including grains in highly altered regions and those at the edges of the thin section, were not considered. Grain size estimates were obtained using both the long axes of ellipses and diameters of circles. Larger grains are more likely to intersect altered regions or the edge of the thin section and are thus more likely to be excluded from the analysis, resulting in underestimation of grain size. To correct for this, we multiplied our measurements of mean grain size by 1.15. This number was obtained by simulating a smaller thin section within the largest traced thin section in the study (50 mm × 75 mm) by drawing a smaller box within the large thin section and comparing grain size of: 1) a subset of grains that lay entirely within the box, excluding grains whose boundaries intersected the edge of the box, and 2) a subset of grains that lay within the box and intersected the boundaries of the box.

Foliation and lineation were difficult to determine by inspection of the drill core because of: a) the physical size of the drill core from Hole 1274A (~7.5 cm in diameter), b) the relatively coarse grain size in the rocks, and c) and the very weak orthopyroxene SPO. We determined the SPO by using the long axis of the best-fit ellipse to find the long axis of each grain, constraining weak SPOs by combining data from multiple thin sections cut in the same orientation. By identifying SPOs in non-parallel planes of observation, we could interpolate the orientation of the three-dimensional foliation in the rock. The SPO strength was quantified using the alignment factor (AF) method of Meurer and Boudreau (1998). SPOs that were statistically indistinguishable from an insufficiently sampled random fabric were not used to constrain the foliation.

### 2.2. Lattice-preferred orientation (LPO)

The majority of lattice-preferred orientation (LPO) data were collected at the University of Wyoming using an HKL Technology Nordlys II Electron Backscatter Diffraction (EBSD) Detector mounted on a JEOL 5800LV scanning electron microscope operating with an accelerating voltage of 20 kV. Electron backscatter patterns (EBSPs) were indexed and processed using HKL Channel5 software. All EBSPs were saved as image files and reprocessed to ensure accuracy in indexing. Some LPO data were acquired at the Australian National University with a Nordlys camera mounted on a tungsten filament JEOL 6400 SEM with 20 kV accelerating voltage, a nominal beam current of 10 nA, and analyzed using the HKL Channel+ software package. See Table S1 in Supplementary Materials for sample-specific information.

A total of 22 thin sections were mapped using EBSD. Grid spacing was determined by grain size and alteration and ranged from 250–350 μm. Orientation maps contain roughly 10–25% indexed data and typically obtained at least one orientation measurement from

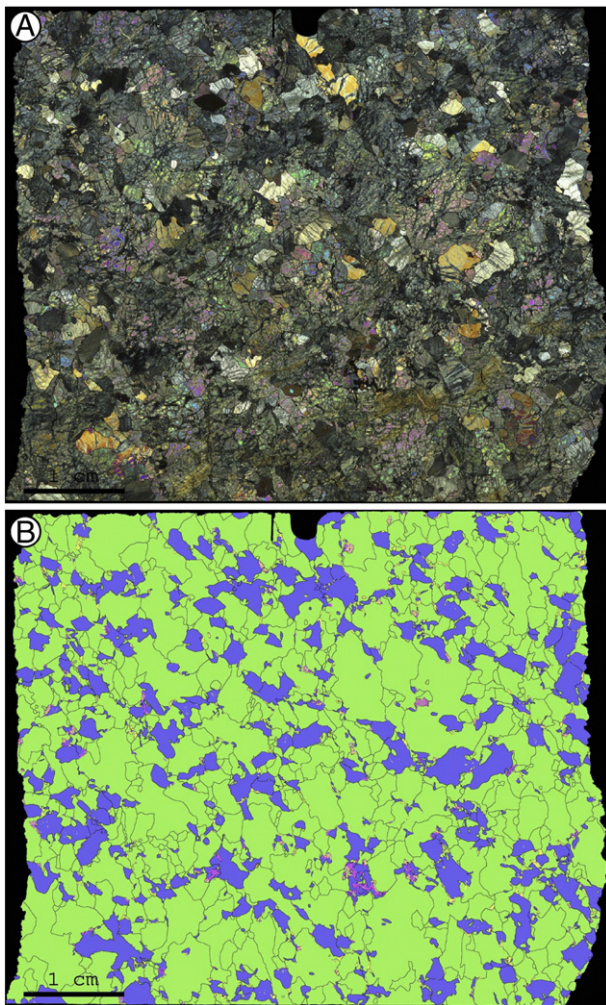


**Fig. 2.** Harzburgite sample 007-53c. A) Crossed polars. B) Grain boundary reconstruction of the sample. Green indicates olivine, blue orthopyroxene, yellow clinopyroxene, and pink spinel.

almost all the grains in the map area. Grains were constrained using the traced images as described in Section 2.1, and were defined as having an angular mismatch  $>10^\circ$ . Most maps contained several thousand orientation data points and sampled ~200–400 grains of olivine and orthopyroxene. Seven thin sections from five additional samples were analyzed manually by EBSD analysis, but no maps were generated. Data collection consisted of hand indexing one data point per grain or relict grain kernel. For these samples, typically 100–200 olivine measurements and 10–40 orthopyroxene measurements were obtained. Only samples with  $>100$  measurements were used, as this is the minimum number required to accurately assess LPO (Ben Ismail and Mainprice, 1998). LPO strength was determined using the M-Index technique (Skemer et al., 2005), as it has been shown to be relatively insensitive to the parameters used in its calculation (Skemer et al., 2005; Wenk, 2002).

The interpretation of EBSD data collected from highly altered abyssal peridotites via orientation mapping is challenging, because LPO data are typically interpreted using one orientation point per grain, while EBSD orientation mapping of crystal orientation in highly altered peridotites yields LPO data that are roughly area-weighted. Our traced thin section images allowed us to extrapolate one-point-per-grain data from four thin sections each in samples 003 and 007 and compare this to “raw” EBSD data, showing that “raw” EBSD LPO data are comparable to one-point-per-grain LPO data in both strength and orientation. This is described in depth in Supplementary information.

### 3. Paleomagnetism: reorienting the samples with respect to each other

The core from Hole 1274A was not recovered as a coherent piece, but rather as a series of discontinuous pieces distributed over 155.8 meters (Section 1). Since the pieces of core were able to spin freely within the core barrel during drilling, and because Hole 1274A was not logged, the azimuthal orientation of each core piece is not known. Paleomagnetic data were used to reorient these samples with respect to: a) each other, and b) their actual configuration adjacent to the MAR.

The magnetic signal in these rocks is carried by magnetite that formed during serpentinization, most likely at temperatures of 250 °C or less (Bach et al., 2004). For all reorientations, we used the paleomagnetic data reported by Garces and Gee (2007).

To place downcore measurements of LPO and SPO in context, individual pieces of core must be oriented relative to each other. Core spinning during drilling should affect paleomagnetic declinations but not inclinations; for this reason, a first-order measure to correct the relative orientations of the core is to align the paleomagnetic declinations to a common orientation (e.g., North). This correction, however, ignores the possibility that faulting subsequent to the magnetization might have caused differential rotation of one part of the core relative to another leading to varying paleomagnetic inclinations downhole. Indeed, the inclinations of the samples included in this study range from 0.6° to 30.4°. Three factors may have caused this variation: a) varying amounts of tectonic rotation in the individual pieces of the core, b) secular variation in the magnetic field during the serpentinization of the core, or c) a drilling overprint of the paleomagnetic vector. Drilling overprint especially is likely to affect the inclinations, as the overprinting adds a vertical component to the magnetic vector and multidomain magnetites such as those found in serpentinized peridotites are more easily overprinted (Morris et al., 2009).

To test whether restoring pieces of the core in Hole 1274A to a common declination is a valid approach, we examined the 4 harzburgite samples mapped by EBSD (Samples 003, 007, 014 and 027), plotting each sample's olivine [100] and [010] maxima along with the magnetic vector measured in the sample (Fig. 3). These samples span nearly the entire length of the core (from ~20 mbsf to

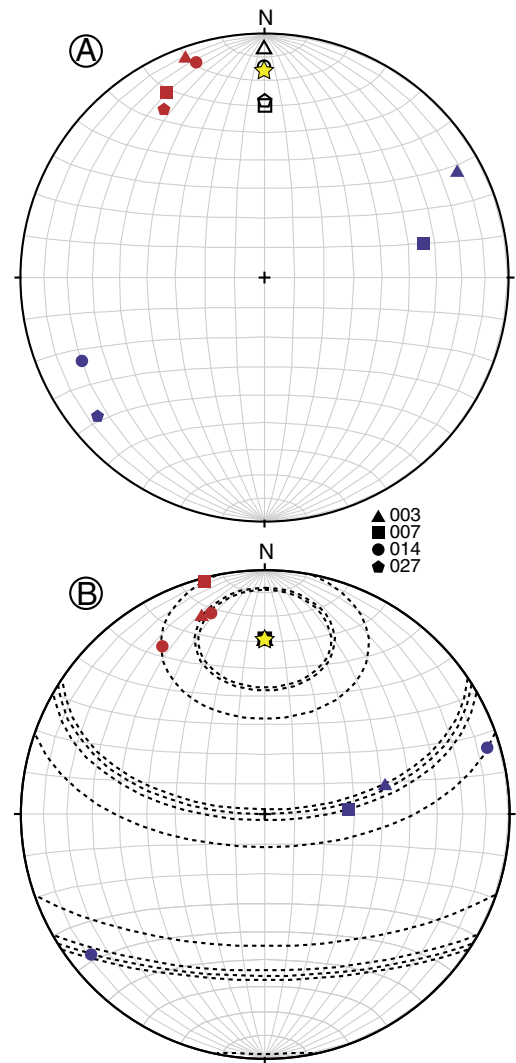


**Fig. 3.** Olivine [100] axis (red) and [010] axis (blue) maxima from the four harzburgite samples analyzed using EBSD orientation mapping (003, 007, 014, 027). Black open symbols indicate the paleomagnetic vectors measured in the samples; yellow star indicates the downcore average paleomagnetic vector. Stereonets are equal-area lower-hemisphere projections, with the drillcore oriented vertically and magnetic north indicated by N. A) Samples reoriented to a common declination, rotated only about a vertical axis parallel to the drillcore. B) Samples reoriented by rotating around an assumed tectonic rotation axis of 330° until individual inclination measurements are at 28°; dashed lines indicate possible locations for the maxima depending on the assumed axis of tectonic rotation.

150 mbsf) and, with 4–5 thin sections analyzed per sample, contain orientation measurements from a very large number of olivine crystals ( $>19,000$  individual orientation measurements in total, ~800–1600 crystals per sample). When the magnetic declinations in the samples are aligned (Fig. 3), the respective mean spherical vectors of the olivine [100] and [010] axis LPO maxima in the four samples are 0.99/1 and 0.92/1 in length, with 95% confidence cones of 10.6° and 30.8°, respectively. (Mean spherical vector is calculated by adding the oriented vectors together, finding the total length of the resultant vector, and normalizing to one, such that perfectly aligned vectors produce a mean spherical vector of 1 and oppositely aligned vectors produce a mean spherical vector of 0.) They are thus very similar in orientation down-core, especially considering the likely natural mineralogical variation in the maximum [100] and [010] orientation from sample to sample, which may be as much as 20° (Skemer, pers. comm.). Furthermore, the angles between the average down-core

paleomagnetic vector and the maximum olivine [100] orientation for each sample do not vary by more than 11°. This observation, and the 10.6° 95% confidence cone for the spherical mean olivine [100] axes, suggests that there is a maximum uncertainty of approximately 11° in alignment between samples, and this is not significant at the resolution required by our study.

An alternative means of reorienting the samples with respect to each other is to assume that the paleomagnetic vectors have not been affected by a vertical drilling overprint or secular variations in the magnetic field, and all the inclination variation is the result of tectonic rotations. In order to reorient the samples, then, an axis of tectonic rotation must be assumed (an issue explored in greater depth in Section 6). One geologically reasonable horizontal rotation axis is 330°, which matches seafloor observations of faulting made by submersible during an ODP site survey cruise (R/V Yokosuka Cruise YK98-05, MODE 98, Leg 1; Casey, pers. comm.). Using this assumed axis of rotation, the four samples shown in Figure 3 must be rotated by 38° (sample 003), 99° (sample 007), 24° (sample 014) and 2° (sample 027), respectively, in order to restore their inclinations to 28°. When this is done, the alignment of the olivine [100] axes does not change appreciably, with a mean spherical vector of .9861/1 (95% confidence cone 12.6°). The olivine [010] axes become substantially less aligned, with a mean spherical vector of .8560/1 (95% confidence cone 44.6°). Reorienting the samples in this way implies variable differential rotations of >90° across ~130 m of drill core, which seems geologically unlikely. An alternative axis of rotation such as 4.5°, the regional trend of the ridge axis, cannot rectify this problem. In such a case, sample 007's inclination of 30.4° cannot reach an inclination of 28° with any amount of rotation about that axis, while the other three samples would require rotations ranging from 25° to 87°. Indeed, if the varying inclinations were to result from tectonic rotations rather than from the errors mentioned above, any assumed axis of rotation would require large sample-to-sample variations in the magnitude of rotations in order to reorient each sample's inclination individually, simply because the samples' inclinations vary so widely. We therefore assume that most of the rotation experienced by these samples *with respect to each other* occurred about a vertical axis during and after drilling (i.e., that the remanent paleomagnetic declinations of our samples were originally aligned in approximately the same direction prior to drilling, and present-day variation in inclination results from sources of error such as drilling overprint and secular variation in the magnetic field during serpentinization). This assumption is also consistent with the relatively minimal evidence for faulting in the core, especially from 0–88 m depth (Fig. 1). Thus, throughout this contribution we will reorient the rocks relative to each other by aligning the paleomagnetic declinations measured in the rocks. Of note, however, is that the orientation of the olivine [100] axes with respect to the sample's individual paleomagnetic vector is consistently at a low angle (Fig. 3b), an observation that is true regardless of the method used to reorient the samples with respect to each other.

Because the *in situ* magnetic declination of the samples is unknown, reorienting the samples with respect to geographic coordinates requires a knowledge of the rotation history of the sample since the magnetic vector was acquired. This is discussed further in Section 6.

#### 4. Microstructure results

Two recent contributions (Seyler et al., 2007; Suhr et al., 2008) discussed the textures and modal compositions of the Hole 1274A peridotites. We concur with their findings, especially that pyroxenes and spinel preserve extensive evidence for pervasive melt-rock interaction. We briefly summarize their results below, alongside our new observations based on grain boundary reconstruction. For purposes of comparison, our modal composition data, calculated

based on the grain boundary reconstruction images, are summarized in Table S2 in Supplementary Information.

##### 4.1. General microstructural description

The Hole 1274A peridotites preserve uniform protogranular (coarse granular) textures. Orthopyroxene occurs mostly as aggregates of large (~1–5 mm) irregularly shaped cusped grains with low aspect ratios. Evidence of dynamic recrystallization is rare; no true neoblasts of orthopyroxene are observed. Orthopyroxene shapes appear to be controlled more by post-kinematic processes (perhaps related to melt percolation) than by deformation.

All spinel and clinopyroxene in the Hole 1274A peridotites appear to be melt-related in origin, either through direct precipitation from melt or through melt-rock reactions (Seyler et al., 2007; Suhr et al., 2008). Both tend to be found as small (<0.05 mm) interstitial grains, or as symplectitic intergrowths.

##### 4.2. Olivine microstructure and grain size distribution (GSD)

Olivine–olivine grain boundaries are irregular and are influenced by significant grain boundary migration. Microstructural evidence for this process includes: a) complex grain shapes with bulging grain boundaries (Figs. 2 and 4A), and b) grain boundary pinning by other phases (Figs. 2 and 4A). Small olivine grains are often elongate and irregularly shaped (Fig. 4A) and are not true neoblasts. Olivine is not in textural equilibrium. Few grain triple junctions are ~120° in the plane of the thin section, and grain shapes are complex, with tortuous grain boundaries and small olivine grains completely engulfed in larger ones (Figs. 2 and 4A).

Olivine grain sizes and grain size distributions (GSDs) were analyzed quantitatively in samples 003 and 007. The mean olivine grain size in these rocks (long axis of best-fitting ellipse) is ~1.5 mm (diameter of an equal-area circle is 0.6 mm). When weighted by area to reflect the volume average, olivine grain size averages ~5.2 mm (diameter of equal-area circle = 1.9 mm). The difference between these two estimates of mean olivine grain size reflects the large number of small grains relative to the fewer number of very large grains, an effect of the skewed GSD. By volume (e.g., the way a seismic wave would experience the rock), most of the sample is comprised of a relatively few number of large grains, and the area-weighted mean olivine grain size reflects this observation. The GSD (Fig. 4B) is intermediate between experimentally deformed olivine aggregates and experimentally deformed and then annealed olivine aggregates (Faul and Scott, 2006). This suggests that the grain size evolution of these samples may have been as follows: 1) during upwelling, olivine deformed and underwent dynamic recrystallization, resulting in the development of numerous small grains, and 2) after dynamic recrystallization ceased, grain growth and textural recovery began but did not continue to equilibrium.

Some smaller olivine grains adjacent to orthopyroxene may be secondary following melt-rock interaction (Seyler et al., 2007; Suhr et al., 2008). This process may have affected the olivine GSD in the rocks, although it is difficult to distinguish it from the effects of grain boundary pinning during annealing. The olivine GSD in these rocks, whether influenced by post-tectonic static annealing or melt-rock reaction or both, cannot have resulted from deformation alone.

##### 4.3. Shape-preferred orientation (SPO)

The very small alignment factors (AFs) determined for the harzburgites confirm that the SPO in these samples is very weak (Fig. 5). Using the statistically significant AFs from the paleomagnetically reoriented samples 003 and 007, we were able to constrain a weak olivine foliation dipping at 82° (Fig. 5). Samples 007, 017 and 027 yielded statistically significant AFs for orthopyroxene, although

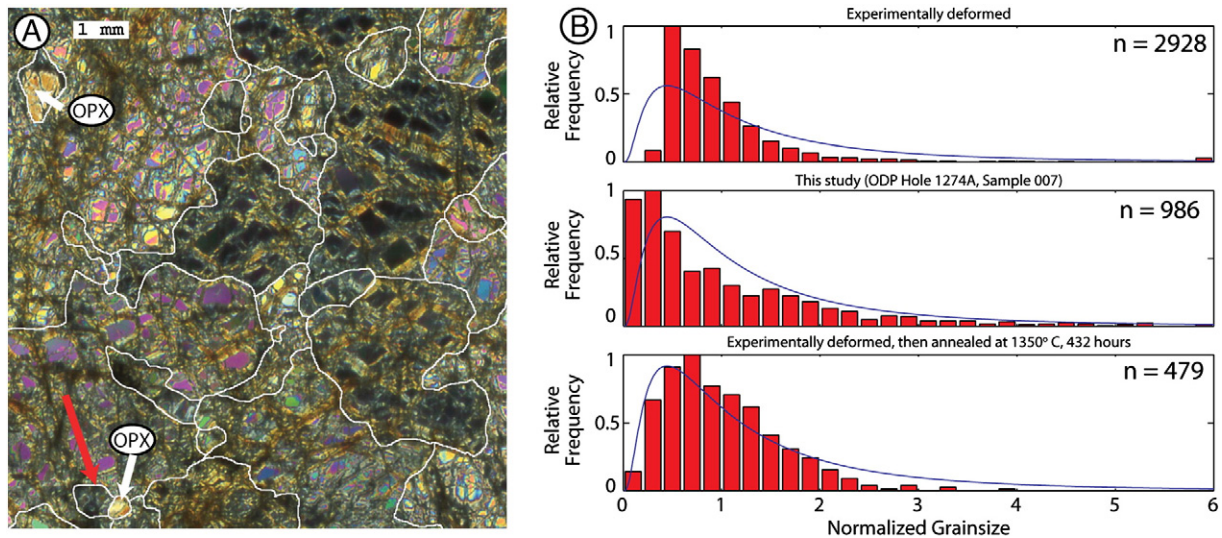


**Fig. 4.** A) Olivine and orthopyroxene from sample 003-116a. All grains in this image are olivine except for the labeled orthopyroxene grains. Note the complex grain boundaries in olivine (outlined in white); they are irregular and bulge into neighboring grains. Red arrow indicates an olivine grain boundary that is pinned by an orthopyroxene grain. Also note the orthopyroxene grain in the upper left that is completely engulfed by an olivine grain. B) Olivine GSDs, binned by grain size normalized to the mean grain size of the sample. Top: Olivine GSD of a sample that has been experimentally deformed and has not annealed. (Average grain size: 101  $\mu\text{m}$  before deformation, 22  $\mu\text{m}$  after deformation) Middle: Olivine GSDs calculated from grain size data combined from sample 007 from Hole 1274A (this study); this GSD is intermediate between that for the deformation and steady-state grain growth experiments. Bottom: Olivine GSD from a sample that has been hydrostatically annealed following experimental deformation; this GSD indicates that the sample has experienced steady-state grain growth. (Average grain size: 33  $\mu\text{m}$ ). Experimental data are from [Faul and Scott \(2006\)](#), measured as described therein. Modeled theoretical GSD is log-normal.

no single plane could be fit through the SPO data ([Fig. 5](#)). Sample 007, with an AF of 19.7, had the strongest orthopyroxene SPO, and over  $45^\circ$  separated its 95% confidence interval from that of sample 017, with its weak but statistically significant AF of 9.3. Thus, a single orthopyroxene foliation could not be determined. Shipboard inspection of the core suggested that the pyroxene foliation in the peridotites from Hole 1274A is extremely weak or absent ([Kelemen et al., 2004](#)). Thus, there may be no consistent orthopyroxene foliation in these rocks. Of note is that in the one case where statistically significant olivine and orthopyroxene SPOs were observed, they differ in orientation by  $\sim 38^\circ$  ( $2\sigma = 28^\circ$ ), suggesting an oblique relationship between the orthopyroxene and olivine foliations.

Most spinel in these rocks occurs as symplectitic intergrowths with clinopyroxene or as complex anhedral aggregates, and is interpreted to have formed from post-deformation melt or melt-rock interactions ([Seyler et al., 2007](#); [Suh et al., 2008](#)). Therefore, the preserved complex shapes cannot have survived any appreciable deformation and do not preserve a kinematic lineation. When clinopyroxene and spinel shapes are combined and analyzed for SPO, samples 003 and 007 yield statistically significant results ([Fig. 6](#)). These SPO results reflect the preferred orientation of either trapped melt products or preferential melt pathways through the rock, or components of both. The majority of this SPO signal appears to be carried by very elongate clinopyroxene (and occasional spinel) that “wets” orthopyroxene grain edges, and by elongate clinopyroxene-spinel symplectites. Of note is that this interpreted melt SPO is intermediate between the olivine SPO and the orthopyroxene SPO (as defined by the well-constrained data from sample 007), but is more similar to the olivine SPO. Melt pathways were most likely controlled by existing grain boundaries, and olivine comprises a greater proportion of these rocks than does orthopyroxene.

The microstructural evidence for melt impregnation and mobile olivine grain boundaries, combined with the olivine GSDs, strongly suggests that these peridotites experienced a period of post-tectonic melt-rock interaction following deformation in the upwelling mantle.

## 5. Lattice-preferred orientation (LPO)

### 5.1. Results

A total of 19 515 olivine crystallographic measurements were made on 23 thin sections from the 9 harzburgites ([Fig. 7](#)). Olivine [010] axes show the strongest maxima, with moderately developed [100] maxima and [001] axes that are only weakly aligned. These data define a weak LPO (average M-index  $\approx 0.1$ ). Orthopyroxene LPO data, based on 8594 measurements on the 9 harzburgites, show strongly developed [001] and [100] maxima, with less strongly aligned [010] axes (average M-index  $\approx 0.1$ ). The olivine crystallographic data from the dunite (sample 008) have a similar orientation to the olivine LPO of the harzburgites. However, because of the very large grain size in the dunites (probably with a volume average  $> 1$  cm, although we do not have a sufficient sample size to make an accurate estimate), we do not have orientation data from a sufficient number of grains to calculate a meaningful M-index.

### 5.2. Interpreting the slip system

To interpret a slip system in olivine and orthopyroxene using these LPO data, we use the olivine foliation defined by the SPO of the samples. We are able to superimpose the SPO data and the LPO data using the paleomagnetic reorientations as discussed in [Section 3](#). Combining the LPO with the SPO-derived olivine foliation ([Fig. 8](#)), it is apparent that olivine [010] and orthopyroxene [100] axes are oriented nearly perpendicular to the foliation. This suggests that the olivine and orthopyroxene must be slipping on the (010) and (100) planes, respectively. However, the slip direction is less clear, because a lineation cannot be recognized in the hand samples. Inspection of the LPO data ([Figs. 7 and 8](#)) reveals that the olivine [100] and orthopyroxene [001] axes appear to be coincident and lie within the plane of the foliation. Thus, the slip systems active in these rocks were most likely (010)[100] in olivine and (100)[001] in orthopyroxene. Because the lineation is not constrained by the hand samples, it is possible that slip directions in olivine and orthopyroxene were [001]

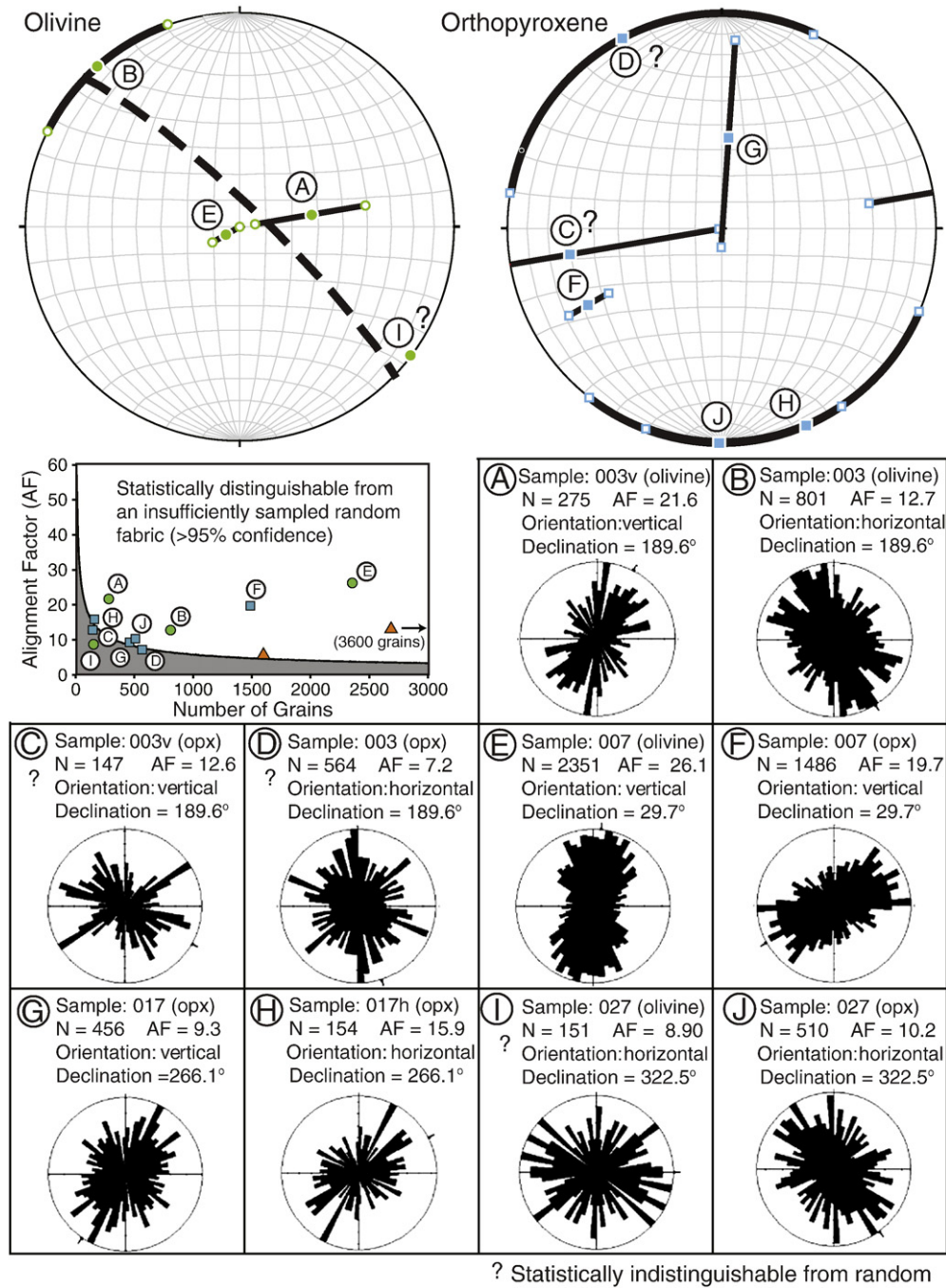


**Fig. 5.** Shape-preferred orientation results from the Hole 1274A peridotites. Pole figure on left is olivine SPO data, with dashed line indicating the best-fit olivine foliation (sample 027 is not included in this calculation; its error bars, not shown, span 180°); right pole figure is orthopyroxene SPO data. Graph indicates the statistical significance of alignment factor (AF) numbers (1 = random, 100 = perfectly aligned). Gray area indicates AFs that are not statistically significant for the number of grains measured. Orange triangles show clinopyroxene-spinel AFs for the SPO data displayed in Fig. 6. A–F) SPO data shown by sample. N indicates number of grains traced. Samples labeled “horizontal” are shown as if looking down on a horizontal slices of core with the paleomagnetic declination plotted at north. Samples labeled “vertical” are shown as slabs as if looking at the face of the working half of the core, although some thin sections (for example, 007–53c shown in Fig. 2.3) may be taken from the “flip side” of the billet. Declinations given indicate the declination of the measured paleomagnetic vector relative to the back of the working half of the core. Paleomagnetic data from [Garces and Gee \(2007\)](#); alignment factor from [Meurer and Boudreau \(1998\)](#). Pole figures are equal-area lower hemisphere projections.

and [010], respectively. However, the (010)[001] slip system in olivine ([Jung and Karato, 2001](#); [Skemer et al., 2006](#)) has only been observed in conditions with high water content, which is not likely in this tectonic setting. Furthermore, the orthopyroxene (100)[010] slip system has not been observed either experimentally or in nature. Thus, we conclude that olivine and orthopyroxene were deformed in the commonly observed (010)[100] and (100)[001] slip systems, respectively.

### 5.3. Relative orientations of the olivine LPO slip direction and the magnetic vector

[Figure 3](#) shows both the orientation of the olivine LPO data and the mean magnetic vector for the samples. Although there is considerable uncertainty in both the magnitude and axis of any tectonic rotation(s) the Hole 1274A peridotites may have experienced, the spherical mean olivine [100] axis maxima in these rocks is only 24.1° (95% confidence

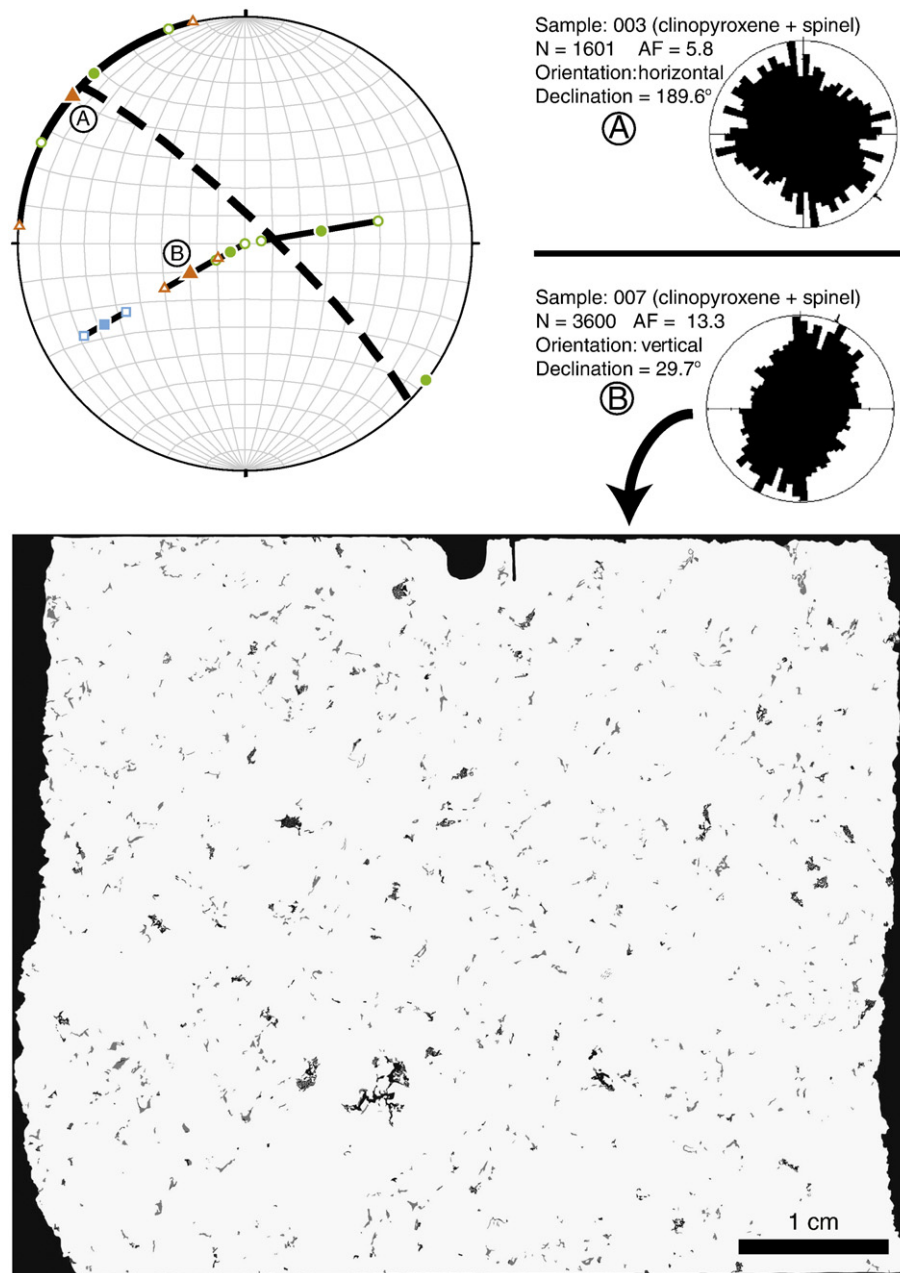


**Fig. 6.** Shape-preferred orientation results from combined spinel and clinopyroxene shapes. Pole figure shows clinopyroxene-spinel SPO results (orange triangles) from samples 003 (A) and 007 (B) relative to the olivine (green circles) and orthopyroxene (blue square) shapes shown in Fig. 5. Orientation of sample 003 rose diagram is shown as if looking down at a horizontal slice of the core; orientation of sample 007 is shown as if looking at a slab from the face of the working half of the core. Declinations are the same as those given in Fig. 5. Bottom image shows combined clinopyroxene (light gray) and spinel (black) shapes from sample 007-53c; image is "flipped" from that shown in Fig. 3 for comparison to rose diagram (original thin section, shown in Fig. 3, is taken in an orientation  $180^\circ$  from the face of the working half of the core). Pole figure is equal-area lower-hemisphere projection.

cone of  $10.6^\circ$ ) from the mean magnetic vector in the core. Thus, any assumed axis of tectonic rotation would still result in the olivine [100] axes located within  $\sim 24.1 \pm 10.6^\circ$  of magnetic north, or to within  $\sim 28.6 \pm 10.6^\circ$  of the ridge axis, which trends  $\sim 4.5^\circ$  East of North (Fig. 9). This observation alone shows that the olivine [100] axes, and hence the preserved mantle flow direction, were at low to moderate angle to the ridge axis when the magnetization was acquired at  $\sim 250^\circ\text{C}$ .

## 6. Undoing low temperature tectonic rotations

Based on the consistent LPO when samples are reoriented to a common declination (Section 3; Fig. 3), we assume that the core from

Hole 1274A represents a fairly coherent block of mantle. To investigate the effects of tectonic rotations on this block of mantle, we have averaged the paleomagnetic inclinations measured our samples, for a mean inclination of  $16.2^\circ$ . This averaging is intended to compensate for errors associated with the magnetic measurements, with the possibility that some multidomain magnetites in the sample were affected by a vertical magnetic overprint acquired during drilling (e.g., Morris et al., 2009), and with the uncertainty associated with secular variation of the magnetic field (Garces and Gee, 2007), as discussed in Section 3. This averaged inclination of  $16.2^\circ$  is comparable to the mean inclination of  $16.5^\circ$  determined by Garces and Gee (2007). Their number was derived by excluding samples interpreted to have been structurally isolated by tectonic rotations.

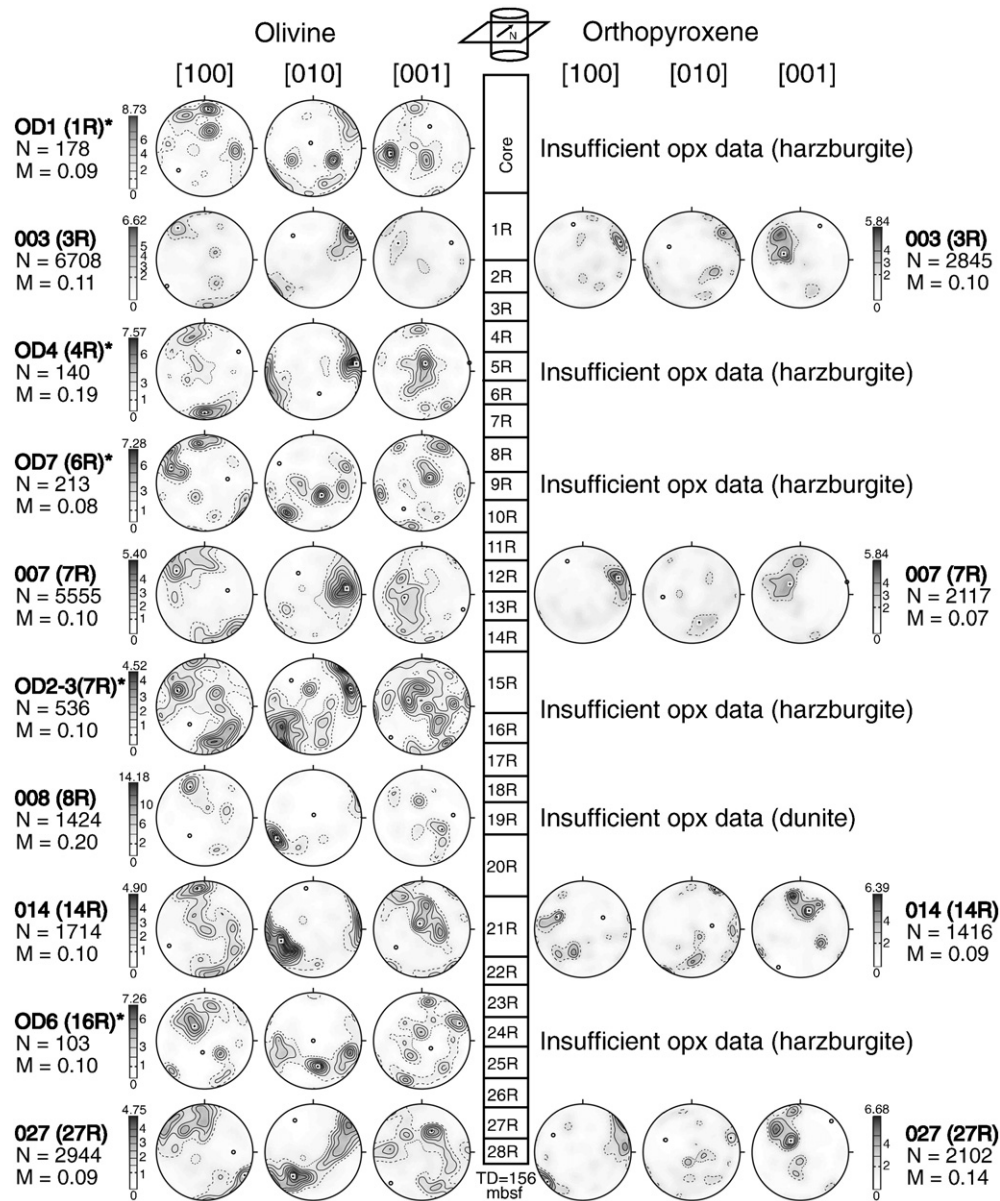


**Fig. 7.** Compiled LPO results from Hole 1274A. Pole figures, generated using the software of Mainprice and Silver (1993) are equal-area lower-hemisphere projections. N indicates the number of data points collected; M indicates M-index (0 = random orientation; 1 = perfect alignment). Contours are shown as multiples of uniform distribution, and are calculated with a half-width of  $8.5^\circ$ . Data have not been processed in any way, and are shown here as they were collected on the EBSD. Asterisks mark samples analyzed at ANU (see Section 2.2 for methodology). Data shown are not one-point-per-grain, though the data are comparable to one-point-per-grain data in both orientation and strength. The data are displayed in an orientation (illustrated schematically) such that the measured declination in the sample is oriented to the north; data are plotted as horizontal “slices” of the core, such that a line with a dip of  $90^\circ$  would be oriented parallel to the direction of drilling.

Using anisotropy of magnetic susceptibility (AMS) as a proxy for foliation/LPO, they excluded samples with AMS diverging by  $>45^\circ$  from the average AMS. Excluded cores include those of samples 003 and 007. These are two of the freshest cores recovered from Hole 1274A, and the unmistakable consistency in our LPO data (Section 3; Figs. 3 and 7) show that these samples can be reoriented relative to each other by rotating them to a common declination. Thus, we choose not to exclude these data, and we use the  $16.2^\circ$  inclination determined by averaging all magnetic data from Hole 1274A.

The orientation of the magnetic inclinations measured in these peridotites indicate that some degree of tectonic rotation has occurred since these rocks acquired their magnetic signature (Garces and Gee, 2007; Kelemen et al., 2004). Unless tectonic rotation occurs about a horizontal axis trending E–W (unlikely in this case, as the ridge axis trends ~N–S), any amount of tectonic rotation that results in a change

of inclination will also affect the declination of the magnetic signal. Because the orientation of the rocks within the horizontal plane is not constrained, we do not know the present-day azimuth of the magnetic declination measured in these rocks (i.e., the divergence of the magnetic declination from true north). Therefore, we do not know the orientation of the axis about which tectonic rotation occurred, nor the magnitude of the tectonic rotation. Thus, to reorient the samples we must assume a geologically reasonable axis of tectonic rotation. Once this assumption has been made, we can use the measured average inclination to “restore” the paleomagnetic declination to its present-day rotated orientation away from magnetic north, and then “undo” the tectonic rotation about the assumed axis until the declination is oriented to magnetic north and the inclination reflects the time-averaged value it should have at this latitude ( $\sim 28^\circ$ ) (Garces and Gee, 2007). All reorientations are performed using a time-averaged geocentric magnetic axial dipole.

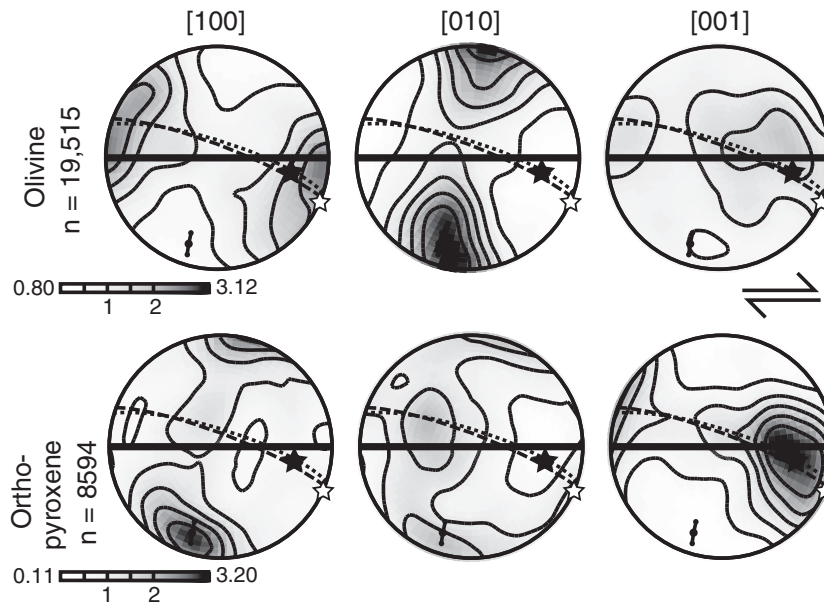


**Fig. 8.** Olivine and orthopyroxene data from samples 003, 007 and 014, plotted in our inferred kinematic reference frame based on the interpreted olivine foliation (heavy black line). White star is best-axis fit to olivine [100] axes, as determined using the software of Mainprice and Silver (1993) and used here as a proxy for lineation, which cannot be observed in these rocks; dotted line is plane perpendicular to best-axis fit to olivine [010] axes. Black star is best-axis fit to orthopyroxene [001] axes; dashed line is plane perpendicular to best-axis fit of orthopyroxene [100] axes. Circles with black bar are the orthopyroxene SPO data point from sample 007 (and error bars) as shown in Fig. 5. Pole figures are lower hemisphere equal-area projections; contours are shown as multiples of uniform distribution, and are calculated with a half-width of  $8.5^\circ$ . Sense of shear, shown by opposing arrows, is for convenience of interpretation only and may well be reversed, as no lineation was observable in the rocks.

In the simplest model, tectonic rotation at a mid-ocean ridge occurs about a horizontal axis parallel to the ridge axis, in a top-away-from-the-ridge direction. Based on bathymetric evidence (Fig. 1), we assume a regional ridge-axis trend of  $4.5^\circ$  E of N. However, bathymetry reveals a large fault scarp nearest to the location of Hole 1274A immediately to the east of the drill site striking  $\sim 350^\circ$ . Observations made by submersible during an ODP site survey cruise (R/V Yokosuka Cruise YK98-05, MODE 98, Leg 1; Casey, pers. comm.) suggest numerous smaller faults in the area striking at  $330^\circ$ . These small-displacement (1–3 m) features occurred late in the uplift history of these rocks, and therefore cannot be responsible for the majority of rotation experienced by these samples. However, it is possible that they reflect a regional stress field similar to that responsible for the large fault visible in the bathymetry, and earlier large-offset faults may have resulted in rotation about similar axes.

Using an average inclination of  $16.2^\circ$  and an assumed horizontal axis of rotation of  $330^\circ$  based on the small fault scarps, we have reoriented the LPO and SPO data from samples 003, 007, 014 and 027. This requires  $\sim 21^\circ$  of rotation to restore the inclination to  $28^\circ$ . Alternatively, using an axis of rotation of  $4.5^\circ$ , consistent with the regional ridge axis trend to the north of the FTFZ, requires a rotation of  $62^\circ$ . This latter rotation seems high, given that the magnetization was acquired at only  $250^\circ\text{C}$ ; consequently we favor a rotation axis of  $330^\circ$  that is consistent with the visible fault scarps seen and the bathymetry. We cannot rule out highly complex tectonic rotations involving multiple episodes of movement around variably oriented rotation axes. However, the rotation that occurred since the acquisition of the magnetic signal at  $250^\circ\text{C}$  is most likely reflected in the bathymetry, whose long ridges and scarps subparallel to the ridge axis (Fig. 1) suggest relatively simple tectonic rotations below  $250^\circ\text{C}$ .

With the data thus reoriented using  $330^\circ$  as the assumed axis of rotation, olivine [100] axes are subhorizontal and subparallel to the ridge axis (Fig. 9). As discussed above, although there is considerable uncertainty in both the magnitude and axis of tectonic rotation, the olivine [100] axis maximum in these rocks is only  $24.1^\circ \pm 10.6^\circ$  from the mean magnetic vector of the rocks. Thus, any assumed axis of tectonic rotation would still result in olivine [100] axes located within

$24.1^\circ \pm 10.6^\circ$  of magnetic north, or  $\leq 28.6^\circ \pm 10.6^\circ$  from the ridge axis (Fig. 9). This observation alone shows that the olivine [100] axes, and hence the mantle flow direction, were definitely oblique to the ridge axes when the magnetization was acquired at  $\sim 250^\circ\text{C}$ .

Olivine [010] axes (i.e., the approximate shear plane) at the time of magnetization are less well constrained because the angle between them and the mean magnetic vector is larger, and therefore the envelope of possible orientations relative to the ridge axis is much larger (Fig. 9B). In other words, our reconstruction of the orientation of the shear plane relative to the ridge axis is highly dependent on our assumptions regarding: a) the orientation of tectonic rotation axes, which are partly constrained by bathymetric observations, and b) the magnitude of tectonic rotations, which are very poorly constrained indeed, as we have no record of tectonic rotations between the cessation of ductile flow at  $\sim 1250^\circ\text{C}$  and the onset of magnetization at  $\sim 250^\circ\text{C}$ .

It is, however, possible to use the assumed axis of tectonic rotation and additional assumptions regarding faulting to speculate on the orientation of the olivine LPO at the time homogeneous mantle flow ceased and tectonic block rotation began. Hole 1274A sits on a fault scarp that presently dips at  $\sim 18^\circ$  (Schroeder et al., 2007). If we assume that this fault is responsible for the tectonic rotations of the Hole 1274A peridotites, and assume that it initiated at a dip angle of  $60^\circ$  (striking at  $330^\circ$  as above), this implies  $42^\circ$  of total rotation. If we rotate our LPO measurements accordingly, olivine [100] axes are shallowly dipping ( $18^\circ$ ) at an oblique angle to the ridge axis ( $331^\circ$  E of N, or  $33.5^\circ$  from the ridge axis), and olivine [010] axes are moderately dipping ( $44.8^\circ$ ) and at high angle to the ridge axis ( $75^\circ$  W of N, or  $70.5^\circ$  from the ridge axis). If our assumptions of orientation and magnitude of tectonic rotation are correct, this implies that the mantle sampled by Hole 1274A may have been flowing along a tilted shear plane in a direction at low angle to the ridge axis at the time homogeneous ductile flow ceased.

## 7. Models of mantle flow

Our data indicate that olivine [100] axes were oriented subparallel to the ridge axis at the time of the serpentinization and the associated

acquisition of the magnetic vector (Sections 5.3 and 6). This is consistent with a 3-D model of mantle flow. However, there is a gap in the recorded rotation history of these rocks. Microstructures observed in this study suggest that homogeneously distributed deformation ceased at  $\sim 1250^\circ\text{C}$  or shortly thereafter, as the rocks have been

affected by pervasive melt-rock interaction and preserve high-temperature LPOs. On the other hand, the magnetic signal in these rocks is carried in magnetite that formed as olivine altered to serpentine at temperatures of  $\sim 250^\circ\text{C}$  or less (Bach et al., 2004). Thus, it seems likely that some tectonic rotation occurred along shear zones and faults after homogeneous ductile deformation ceased but before the onset of serpentinization, and any amount of tectonic rotation calculated using paleomagnetic data must be regarded as a minimum value – most likely only a fraction of the total amount of tectonic rotation.

Given this limitation the simplest model of tectonic rotations in these rocks—that is, top-away-from-the-ridge rotation on faults striking parallel to the ridge axis—seems impossible. As mentioned above, using a ridge axis orientation of  $4.5^\circ\text{E}$  of N, rotation along faults parallel to the ridge axis requires  $\sim 62^\circ$  of tectonic rotation after the rocks cooled to  $250^\circ\text{C}$ . This result seems to imply very high amounts ( $>200^\circ$ ) of total rotation given that the majority of rotation between  $1250^\circ\text{C}$  to  $0^\circ\text{C}$  most likely occurred above  $250^\circ\text{C}$ , and this amount of rotation is geologically unreasonable, as simple “corner flow” would result in a total of only  $\sim 90^\circ$  of tectonic rotation (e.g., Schroeder et al., 2007). Therefore the hypothesis that all the rotation occurred about an axis parallel to the ridge seems to be unlikely.

Four models of mantle flow and tectonic rotation can explain the observed data (Fig. 10). Here we consider each of these in turn.

#### 7.1. Model 1: 3-D mantle flow and subsequent tectonic rotation subparallel to the ridge axis

The olivine LPO we observe show that olivine [100] axes were at low angle to the ridge axis at the time the rocks acquired their magnetization at  $250^\circ\text{C}$  (Fig. 9A). This well-constrained observation alone is consistent with a 3-D model of mantle flow. If all tectonic rotation took place about an axis parallel or subparallel to the ridge axis, the olivine flow direction must have been subparallel to the ridge at the time the rocks accreted to the lithosphere and began rotation as a tectonic block. This condition is required by the low angle between: a) olivine [100] axes, b) the magnetic vector in the rocks, and c) the ridge axis (Fig. 9). Any model incorporating tectonic rotations about bathymetrically observable sub-ridge-parallel faults requires 3-D flow in the mantle (Fig. 10A).

This model of mantle flow is not completely satisfactory. Reorienting the olivine [010] axis to their possible orientation at the time of the onset of tectonic rotations (Fig. 9C) suggests that the shear plane may not have been horizontal. This is inconsistent with a 3-D model of mantle flow. Furthermore, numerical models (e.g., Blackman and Forsyth, 1992; Blackman et al., 2002) and observations from ophiolites (Boudier and Nicolas, 1995; Ceuleneer and Rabinowicz, 1992; Ceuleneer et al., 1988; Jousset et al., 1998) suggest that corner flow directly beneath the ridge axis probably happens very close to the crust-mantle boundary. To exhume peridotites to the seafloor, the

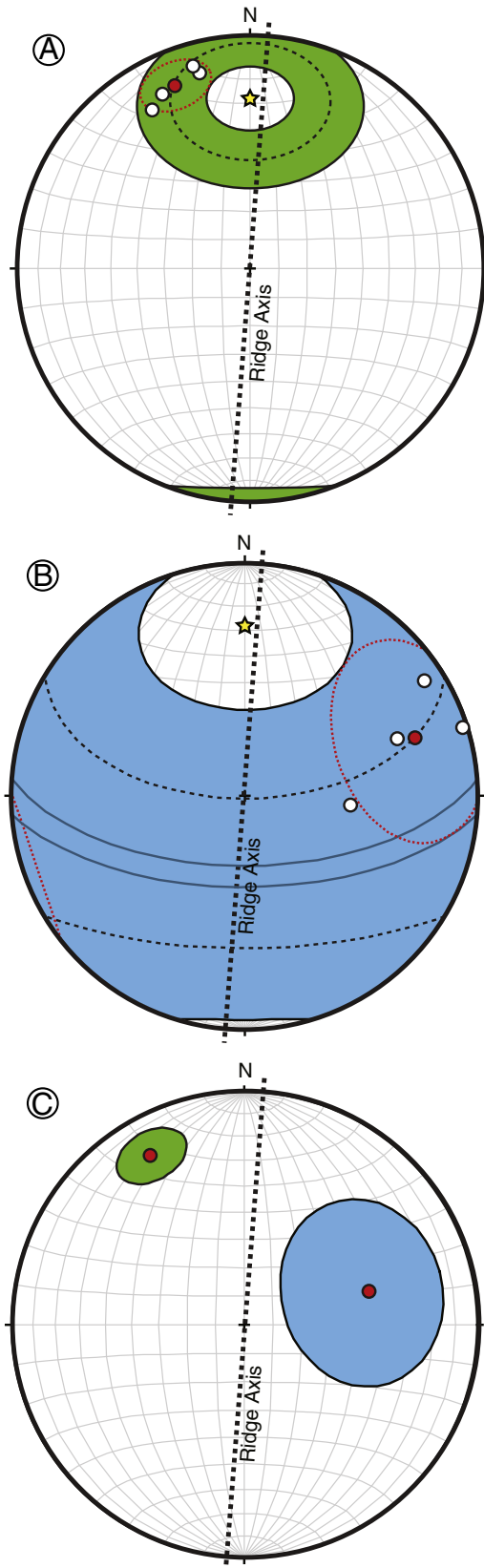


**Fig. 9.** A) Pole figure illustrating the possible locations of olivine [100] axis maxima relative to the average magnetic vector (yellow star) after “undoing” the tectonic rotations that have occurred since the acquisition of the magnetic signal. Regardless of the axis of tectonic rotation, the angle between the average magnetic vector measured in the samples (inclination of  $16.2^\circ$ ) and the olivine [100] axes ( $24.1^\circ$  from magnetic vector, with the  $10.6^\circ$  95% confidence cone shown as small dashed ellipse) in those samples will remain constant. Thus, olivine [100] axes must have lain somewhere within the green ring at the time the magnetic signal was acquired. White dots show the location of the olivine [100] axes reoriented using the assumed axis of tectonic rotation that we prefer ( $330^\circ$ ); red dot is the mean vector for the four data points. B) Pole figure as above, for olivine [010] axes. C) A possible orientation for olivine [100] (green) and [010] (blue) axes (mean vectors shown as red dots) at the time of the cessation of homogeneous deformation in the mantle. This orientation “undoes”  $42^\circ$  of total tectonic rotation about an assumed tectonic rotation axis of  $330^\circ$ , for a fault initiation angle of  $60^\circ$ . Projections are equal-area lower hemisphere, and sample maxima were calculated using the “best axis” feature of the software by Mainprice and Silver (1993).

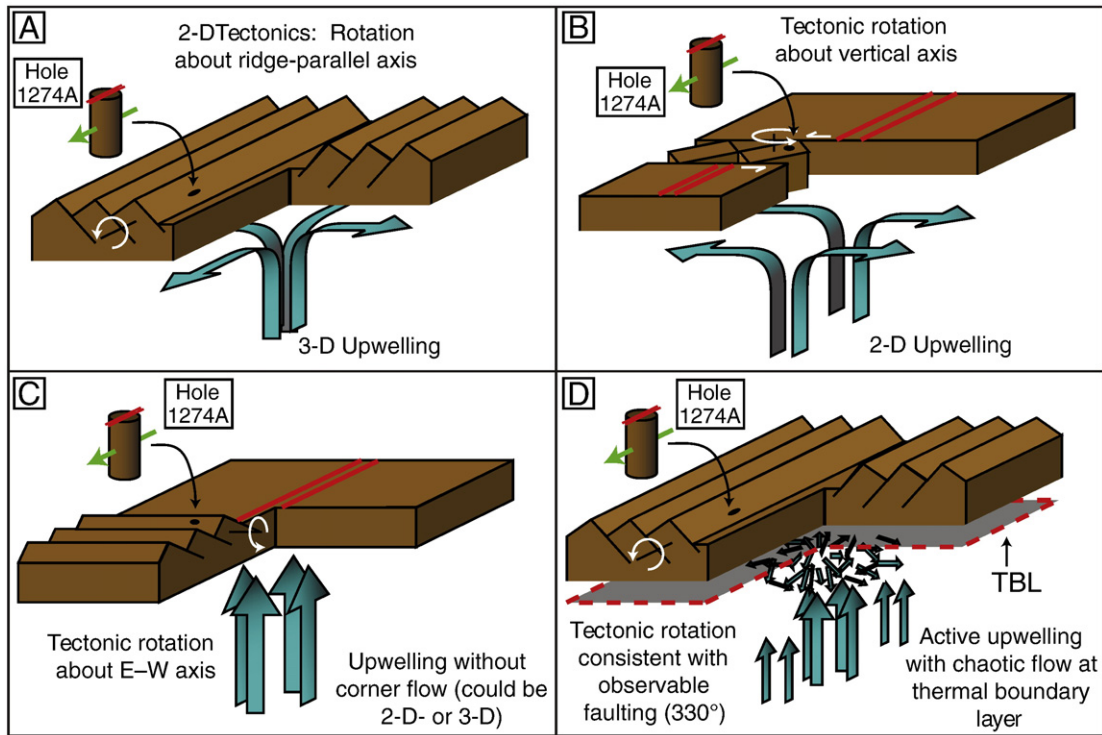


**Fig. 10.** Four possible interpretations of the Hole 1274A olivine orientation data. Hole 1274A is represented schematically in each panel, with the green arrow showing the approximate olivine [100] axes in the drill core and a double red line as the approximate orientation of the ridge axis relative to the LPO. A) 3-D upwelling and corner flow followed by 2-D tectonics. Uplift to the seafloor and associated tectonic rotations accomplished about a roughly ridge-parallel axis. B) 2-D upwelling and corner flow followed by complex tectonic rotations about a vertical axis. C) Upwelling (3-D or 2-D) but no corner flow. Uplift to the seafloor and associated tectonic rotations accomplished about an axis striking E-W (roughly perpendicular to the ridge axis). D) A modified 3-D upwelling scenario: active upwelling focused near segment center, followed by chaotic flow as the actively upwelling mantle encounters cooling (and hence no longer actively upwelling) mantle material in the thermal boundary layer. Uplift to the seafloor and associated tectonic rotations could be accomplished via 2-D or 3-D tectonics; we prefer a rotation axis of  $330^\circ$ , as this is consistent with observable faults in the region. The thermal boundary layer (TBL) is taken here to mean the transition between active upwelling and passive tectonic rotation; its thickness is illustrated schematically and will depend on the depth at which active upwelling ceases and the depth of onset of localized deformation.

lithosphere must be thick, perhaps 10–20 km thick in this area (Kelemen et al., 2007; Schroeder et al., 2007). In the case of magma-starved ridge segments such as this portion of the MAR, where mantle rocks are exhumed directly to the seafloor, it seems likely that the depth of the lithosphere may prohibit high-temperature, homogeneously distributed corner flow in the mantle directly beneath the ridge axis, and “corner flow” may instead be accommodated along shear zones and faults (Kelemen et al., 2007; Schroeder et al., 2007). This is consistent with the recovery of a single peridotite mylonite at the top of Hole 1274A hypothesized by Kelemen et al. (2004) to be a remnant of the high-temperature shear zone responsible for exhuming these rocks to the seafloor, and with bathymetric (Schroeder et al., 2007) and paleomagnetic (Garces and Gee, 2007) observations of this region which suggest large rotated faults. Thus, 3-D flow in this region of the mantle may be unlikely.

#### 7.2. Model 2: 2-D mantle flow and subsequent tectonic rotation about a sub-vertical axis

This model requires that the Hole 1274A peridotites experienced corner flow such that olivine [100] axes were oriented subhorizontally and perpendicular to the ridge axis at the time that tectonic rotation began. To transform subhorizontal ridge-perpendicular olivine [100] axes to the subhorizontal ridge-parallel orientation required by our data, tectonic rotation would have had to have occurred about a subvertical axis. This is not likely given the stresses typically extant at mid-ocean ridge settings away from transform faults. A non-transform discontinuity has been inferred by Fujiwara et al. (2003) six kilometers to the south of Hole 1274A. Deformation associated with this non-transform discontinuity may have influ-

enced tectonic rotations in the region and allowed for rotations about axes that are subvertical (Fig. 10B). However, there is no bathymetric evidence of faults that could accomplish tectonic rotations such as these. The long, approximately ridge-parallel scarps and valleys evident on the seafloor (Fig. 1) suggest tectonic rotations along approximately ridge-parallel axes.

The speculative reorientation of the olivine [010] axes may provide an additional constraint. Like the 3-D model of mantle flow, a 2-D model also predicts an approximately horizontal shear plane following corner flow. Olivine [010] axes were shallowly dipping at the time of magnetization (Figs. 3 and 9), implying a steeply dipping shear plane, and any rotation about a vertical axis would be unable to transform a steeply dipping shear plane into the subhorizontal shear required by a 2-D model of mantle flow. Thus, Model 2 is not our preferred model.

Notably, some seismic observations (Dunn et al., 2005; Toomey et al., 2007) suggest mantle flow directions may be oblique to the spreading direction, perhaps by as much as  $38^\circ$ . This is essentially a rotated 2-D model (although it does not preclude a component of 3-D flow). This is unlikely to be the case here, as: a) the olivine [100] axes we observe were most likely  $>60^\circ$  oblique to the spreading direction at the time of accretion to the lithosphere, b) attempted reorientation of the olivine [010] axes suggest that a horizontal shear plane is unlikely, and c) the thick lithosphere in this region implies that homogeneous ductile corner flow in the mantle is unlikely.

#### 7.3. Model 3: no mantle corner flow and subsequent tectonic rotation about an E-W axis

As mentioned in Section 7.1, the thick lithosphere thought to exist in this region suggests that corner flow in the mantle may have been

accommodated by shearing and faulting rather than by homogeneous ductile flow (Schroeder et al., 2007). Furthermore, observations in ophiolites (e.g., Boudier and Nicolas, 1995; Ceuleneer et al., 1988; Dijkstra et al., 2003; Jousset et al., 1998; Suhr, 1993) suggest that protogranular, melt-influenced microstructures such as those observed in the Hole 1274A peridotites most likely form in conditions of very low differential stress such as those in the upwelling mantle.

LPOs consistent with vertical flow may be preserved in these rocks (Fig. 10C). However, given the relative orientations of the LPO and the paleomagnetic vector (suggesting ridge-parallel subhorizontal olivine [100] axes at  $\sim 250^\circ\text{C}$ ), pre-serpentinization tectonic rotations are required to have occurred about an axis striking close to E–W. Once again, there is no bathymetric evidence for faults striking in this orientation (Fig. 1).

#### 7.4. Model 4: chaotic mantle flow in the TBL and subsequent tectonic rotation consistent with observable faulting

None of the above hypotheses – 3-D flow with ridge-parallel faulting, or 2-D or vertical flow with complex faulting – are entirely satisfactory. Models 1 and 2 require ductile corner flow, which seems unlikely in a region with lithosphere up to 20 km thick (Kelemen et al., 2007; Schroeder et al., 2007), and Models 2 and 3 require faulting that is not consistent with the observed bathymetry of scarps sub-parallel to the ridge axis. Vertical flow, whether focused in 3-D or not, with complex faulting is perhaps the most geologically reasonable in terms of process and microstructural observations, although the fault strike we observe ( $330^\circ$ ) cannot transform vertical olivine [100] axes into an approximately horizontal and ridge-parallel configuration. Additional faults (not bathymetrically observed) would be required. Furthermore, vertical flow is not supported by the speculative olivine [010] axis reorientation (Fig. 9C). Thus, we explore one final possibility to explain the olivine LPO orientations preserved in the Hole 1274A peridotites—a modified 3-D flow hypothesis. Numerical models have shown that active 3-D upwelling is in part hypothesized to develop as a result of buoyancy forces related to melting, provided the mantle viscosity is low, the permeability for melt transport is low, and the spreading rate is slow (e.g., Choblet and Parmentier, 2001; Lin and Phipps Morgan, 1992). Studies in the Oman ophiolite (e.g., Jousset et al., 1998), interpreted to preserve actively upwelling “diapirs” with 3-D flow, suggest that buoyancy drives upwelling directly into the base of the crust-mantle boundary, where a zone of chaotic flow exists before flow transitions to a radial horizontal pattern away from the edges of the upwelling zone. At  $15^\circ\text{N}$  no discrete crust exists to serve as a “hard lid” to stop active upwelling in the manner observed in the Oman ophiolite. Thus, if 3-D active upwelling does occur at depth beneath the MAR, the mantle must at some point transition from active upwelling at very high temperatures to passive tectonic rotations at shallow depths. This transitional zone within the thermal and rheological boundary layer may involve very complex flow in the mantle. If this process occurred, the rocks preserve neither 2-D nor 3-D mantle flow, but rather preserve chaotic flow “frozen in” as the mantle transitioned from active 3-D upwelling to passive 2-D uplift (Fig. 10d). This is consistent with our proposed reorientation of the olivine LPO, with shallowly dipping ridge-subparallel olivine [100] axes and olivine [010] axes dipping moderately and at high angle to the ridge axis at the time of lithosphere accretion. Following the accretion of the rocks to the lithosphere, tectonic rotations along a fault striking  $330^\circ$  may have occurred during uplift to the seafloor. This model could be consistent with a hypothesis put forward by Godard et al. (2008), who suggested that one mechanism for the extreme melt depletion observed in the Hole 1274A mantle may have been complex microconvection at the base of the lithosphere, although it does not preclude alternative models of ancient melt depletion (Harvey et al., 2006; Seyler et al., 2007; Suhr et al., 2008).

## 8. Conclusions

Peridotites drilled from the MAR during ODP Leg 209 preserve olivine and orthopyroxene LPOs consistent with deformation at high temperature ( $\sim 1250^\circ\text{C}$ ) beneath a mid-ocean ridge. The weak crystallographic fabrics (M-index  $\approx 0.1$ ) and melt-influenced protogranular microstructures observed are similar to those found in the upwelling zone of ophiolites and to those predicted by numerical models for upwelling zones, suggesting that corner flow may not have occurred in the mantle directly beneath the ridge axis. Reorientation of the fabrics from Hole 1274A using paleomagnetic data suggests that peridotites beneath this portion of the MAR had an olivine a-axis maximum oriented subhorizontally and at low angle ( $\leq 28.6^\circ \pm 10.6^\circ$ ) to the ridge axis at the time of magnetization. This is consistent with complex 3-D flow in the mantle followed by tectonic exhumation along ridge-parallel faults, or with 2-D mantle upwelling followed by complex 3-D tectonic emplacement. Both scenarios require some 3-D complexity, either in the asthenosphere or in the lithosphere.

Supplementary materials related to this article can be found online at doi:10.1016/j.epsl.2010.10.041.

## Acknowledgements

This work was funded in part by a Geological Society of America Graduate Student Research Grant and by a grant from the Joint Oceanographic Institutions – U.S. Science Support Program to Cheadle. The first author wishes also to acknowledge support by the University of Wyoming Graduate School and the U.W. Department of Geology & Geophysics William H. and Constance C. Spears Fellowship. Thanks to Phil Skemer, Jessica Warren and Doug Toomey for thoughtful and helpful reviews.

## References

- Bach, W., Garrido, C.J., Paulick, H., Harvey, J., Rosner, M., 2004. Seawater-peridotite interactions: first insights from odp leg 209, mar  $15^\circ\text{N}$ . *Geochem. Geophys. Geosyst.* 5.
- Ben Ismail, W., Mainprice, D., 1998. An olivine fabric database: an overview of upper mantle fabrics and seismic anisotropy. *Tectonophysics* 296 doi: 1000141-1000143.
- Blackman, D., Forsyth, D.W., 1992. The Effects of Plate Thickening on Three-Dimensional, Passive Flow of the Mantle Beneath Mid-Ocean Ridges. In: Phipps Morgan, J., Blackman, D., Sinton, J. (Eds.), *Mantle flow and melt generation at mid-ocean ridges*. Geophysical monograph, 71. American Geophysical Union, Washington, D.C.
- Blackman, D.K., Wenk, H.-R., Kendall, J.-M., 2002. Seismic anisotropy of the upper mantle 1. Factors that affect mineral texture and effective elastic properties. *Geochem. Geophys. Geosyst.* 3.
- Boudier, F., Nicolas, A., 1995. Nature of the moho transition zone in the oman ophiolite. *J. Petrol.* 36, 777–796.
- Ceuleneer, G., Cannat, M., 1997. High-Temperature Ductile Deformation of Site 920 Peridotites. In: Karson, J.A., Cannat, M., Miller, D.J., Elthon, D. (Eds.), *Proc. ODP, sci. Results*, 153. Ocean Drilling Program, College Station, TX, pp. 23–34.
- Ceuleneer, G., Rabinowicz, M., 1992. Mantle Flow and Melt Migration Beneath Ocean Ridges: Models Derived from Observations in Ophiolites. In: Phipps Morgan, J.B., Blackman, D.K., Sinton, J.M. (Eds.), *Mantle flow and melt generation at mid-ocean ridges*. Geophysical monographs, 71. American Geophysical Union, pp. 123–154.
- Ceuleneer, G., Nicolas, A., Boudier, F., 1988. Mantle flow patterns at an oceanic spreading centre: the oman peridotite record. *Tectonophysics* 151, 1–26.
- Choblet, G., Parmentier, E.M., 2001. Mantle upwelling and melting beneath slow spreading centers: effects of variable rheology and melt productivity. *Earth Planet. Sci. Lett.* 184, 589–604.
- Dick, H.J.B., 1989. Abyssal Peridotites, Very Slow Spreading Ridges and Ocean Ridge Magmatism. In: Saunders, A.D., Norry, M.J. (Eds.), *Magmatism in the ocean basins*. Special publication, 42. Geological Society of London, London, pp. 71–105.
- Dijkstra, A.H., Barth, M.G., Drury, M.R., Mason, P.R.D., Vissers, R.L.M., 2003. Diffuse porous melt flow and melt-rock reaction in the mantle lithosphere at a slow-spreading ridge: a structural petrology and la-icp-ms study of the othris peridotite massif (greece). *Geochem. Geophys. Geosyst.* 4.
- Dunn, R.A., Lekić, V., Detrick, R.S., Toomey, D.R., 2005. Three-dimensional seismic structure of the mid-atlantic ridge ( $35^\circ\text{N}$ ): evidence for focused melt supply and lower crustal dike injection. *J. Geophys. Res.* 110.
- Escartin, J., Cannat, M., 1999. Ultramafic exposures and the gravity signature of the lithosphere near the fifteen-twenty fracture zone (mid-atlantic ridge,  $14^\circ\text{N}$ – $16.5^\circ\text{N}$ ).
- Faul, U., Scott, D., 2006. Grain growth in partially molten olivine aggregates. *Contrib. Mineralog. Petrol.* 151, 101–111.

- Fujiwara, T., Lin, J., Matsumoto, T., Kelemen, P., Tucholke, B.E., Casey, J.F., 2003. Crustal evolution of the mid-atlantic ridge near the fifteen-twenty fracture zone in the last 5 ma. *Geochem. Geophys. Geosyst.* 4, 1024 doi:10.1029/12002GC000364.
- Garces, M., Gee, J.S., 2007. Paleomagnetic evidence of large footwall rotations associated with low-angle faults at the mid-atlantic ridge. *Geology* 35, 279–282.
- Godard, M., Lagabrielle, Y., Alard, O., Harvey, J., 2008. Geochemistry of the highly depleted peridotites drilled at ODP sites 1272 and 1274 (Fifteen-Twenty Fracture Zone, Mid-Atlantic Ridge): implications for mantle dynamics beneath a slow spreading ridge. *Earth Planet. Sci. Lett.* 267, 410–425.
- Harvey, J., Gannoun, A., Burton, K.W., Rogers, N.W., Alard, O., Parkinson, I.J., 2006. Ancient melt extraction from the oceanic upper mantle revealed by re-os isotopes in abyssal peridotites from the mid-atlantic ridge. *Earth Planet. Sci. Lett.* 244, 606–621.
- Jousselin, D., Nicolas, A., Boudier, F., 1998. Detailed mapping of a mantle diapir below a paleo-spreading center in the oman ophiolite. *J. Geophys. Res.* 103, 18153–18170.
- Jung, H., Karato, S.-I., 2001. Effects of water on dynamically recrystallized grain-size of olivine. *J. Struct. Geol.* 23, 1337–1344.
- Kelemen, P., Kikawa, E., Miller, D.J., Party, S.S., 2004. Proc. ODP, initial reports. Ocean Drilling Program, College Station, TX. doi:10.2973/odp.proc.ir.2209.2004.
- Kelemen, P., Kikawa, E., Miller, D.J., Party, S.S., 2007. Leg 209 Summary: Processes in a 20-km-Thick Conductive Boundary Layer Beneath the Mid-Atlantic Ridge, 14°–16°N. In: Kelemen, P., Kikawa, E., Miller, D.J. (Eds.), *Proceedings of the ocean drilling program, scientific results 209*. Ocean Drilling Program, College Station, TX, pp. 1–33.
- Kuo, B.-Y., Forsyth, D.W., 1988. Gravity anomalies of the ridge-transform system in the south atlantic between 31° and 34.5°S: upwelling centers and variations in crustal thickness. *Mar. Geophys. Res.* 10, 205–232.
- Lawrence, R.M., Gee, J.S., Karson, J.A., 2002. Magnetic anisotropy of serpentinized peridotites from the mark area: implications for the orientation of mesoscopic structures and major fault zones. *J. Geophys. Res.* 107.10.1029/2000JB000007.
- Lin, J., Phipps Morgan, J., 1992. The spreading rate dependence of three-dimensional mid-ocean ridge gravity structure. *Geophys. Res. Lett.* 19, 13016.
- Lin, J., Purdy, G.M., Schouten, H., Sempere, J.-C., Zervas, C., 1990. Evidence from gravity data for focused magmatic accretion along the mid-atlantic ridge. *Nature* 344, 627–632.
- Mainprice, D., Silver, P., 1993. Constraints on the interpretation of teleseismic sks observations from kimberlite nodules from the subcontinental mantle. *Phys. Earth Planet. Int.* 78, 257–280.
- Meurer, W., Boudreau, A., 1998. Compaction of igneous cumulates. Part ii. Quantitative analysis of mineral laminations in the stillwater complex, Montana. *J. Geol.* 293–304.
- Morris, A., Gee, J.S., Pressling, N., John, B.E., MacLeod, C.J., Grimes, C.B., Searle, R.C., 2009. Footwall rotation in an oceanic core complex quantified using reoriented integrated ocean drilling program core samples. *Earth Planet. Sci. Lett.* 287, 217–228.
- Nicolas, A., Rabinowicz, M., 1984. Mantle Flow Pattern at Oceanic Spreading Centres: Relation with Ophiolitic and Oceanic Structures. In: Gass, I.G., Lippard, S.J., Shelton, A.W. (Eds.), *Ophiolites and oceanic lithosphere*. : Special publication, 13. Geol. Soc. London, pp. 147–151.
- Nicolas, A., Violette, J.F., 1982. Mantle flow at oceanic spreading centers: models derived from ophiolites. *Tectonophysics* 81, 319–339.
- Rasband, W.S., 1997–2007. ImageJ. U.S. National Institutes of Health, Bethesda, Maryland, USA.
- Schroeder, T., Cheadle, M.J., Dick, H.J.B., Faul, U., Casey, J., Kelemen, P., 2007. Nonvolcanic seafloor spreading and corner-flow rotation accommodated by extensional faulting at 15°N on the mid-atlantic ridge: a structural synthesis of odp leg 209. *Geochem. Geophys. Geosyst.* 8.10.1029/2006GC001567.
- Seyler, M., Lorand, J.-P., Dick, H.J.B., Drouin, M., 2007. Pervasive melt percolation reactions in ultra-depleted refractory harzburgites at the mid-atlantic ridge, 15° 20' N: ODP hole 1274a. *Contrib. Min. Petrol.* 153, 303–319 doi: 310.1007/s00410-00006-00148-00416.
- Skemer, P., Katayama, I., Jiang, Z., Karato, S., 2005. The misorientation index: development of a new method for calculating the strength of lattice-preferred orientation. *Tectonophysics* 411, 157–167.
- Skemer, P., Katayama, I., Karato, S.-I., 2006. Deformation fabrics of the cima di gagnone peridotite massif, central alps, switzerland: evidence of deformation at low temperatures in the presence of water. *Contrib. Min. Petrol.* 152, 43–51.
- Suhr, G., 1993. Evaluation of upper mantle microstructures in the table mountain massif (bay of islands ophiolite). *J. Struct. Geol.* 15, 1237–1292.
- Suhr, G., Kelemen, P., Paulick, H., 2008. Microstructures in hole 1274a peridotites, odp leg 209, mid-atlantic ridge: tracking the fate of melts percolating in peridotite as the lithosphere is intercepted. *Geochem. Geophys. Geosyst.* 9, 1–23.
- Tolstoy, M.A., Harding, J.A., Orcutt, J.A., 1993. Crustal thickness at the mid-atlantic ridge: bull's eye gravity anomalies and focused accretion. *Science* 262, 726–729.
- Toomey, D.R., Jousselin, D., Dunn, R.A., Wilcock, W.S.D., Detrick, R.S., 2007. Skew of mantle upwelling beneath the east pacific rise governs segmentation. *Nature* 446, 409–414.
- Tucholke, B.E., Lin, J., Kleinrock, M.C., Tivey, M.A., Reed, T.B., Goff, J., Jaroslow, G., 1997. Segmentation and crustal structure of the western mid-atlantic ridge flank, 25°25'–27°10'N and 0–29 m.y. *J. Geophys. Res.* 102, 10203–10223.
- Wang, Y., Forsyth, D.W., Savage, B., 2009. Convective upwelling in the mantle beneath the gulf of california. *Nature* 462, 499–501.
- Wenk, H.-R., 2002. Texture and Anisotropy. In: Karato, S.-I., Wenk, H.-R. (Eds.), *Plastic deformation of minerals and rocks*. Mineralogical Society of America and Geochemical Society, Washington, DC.
- Whitehead, J.A., Dick, H.J.B., Schouten, H., 1984. A mechanism for magmatic accretion under spreading centers. *Nature* 312, 146–148.